Multi-port Macromodeling Method of Thin-wire Structure System based on PEEC Method and Open-circuit Suppression Method

Xin Liu*[1], Xiang Cui[2]

School of Electrical and Electronic Engineering, North China Electric Power University

Yonghua North Street 619, Baoding, Hebei Province, China

*[1]liuxinhust@163.com

Abstract

A multi-port macromodeling method of the thin-wire structure system is proposed in this paper. In this method, the impedance and the admittance of the conductors are calculated using the partial element equivalent circuit (PEEC) method and the node voltage equation is achieved based on the node voltage method. In order to reduce the order of the model, the open-circuit suppression method is adopted. Making use of the vector fitting (VF) method and backward difference method, a time domain solution is achieved. The proposed method is validated by comparing its results with the calculated or measured ones published in other papers. Finally, an application about the direct lightning overvoltage in high-speed railway system is implemented.

Keywords

Partial Element Equivalent Circuit; Open-circuit Suppression Method; Multi-port Macromodeling Method; Thin-wire System

Introduction

The grounding grid, tower of the transmission line, and lightning protection system in the railway system can be viewed as a thin-wire system, which should be modeled in order to calculate the overvoltage due to the direct or indirect lightning striking. Many methods has been proposed to model the thin-wire structure system by using the method of moments (MOM), the finite-difference time-domain (FDTD) method, the hybrid electromagnetic model and transmission line approaches. Recently, the partial element equivalent circuit (PEEC) is adopted to analyzing the thin-wire structure such as grounding grid and lightning protection system. In some complex thin-wire structure such as the transmission line tower or the integrated grounding system in the high-speed railway system, the number of the conductors is very large which will result in a high order of the model and inefficient computation. In order to handle this problem, the open-circuit suppression method is adopted to eliminate the internal nodes, as a result, a multi-port circuit according to the external nodes is built. In the section II of this paper, the modified image method and the PEEC method is presented. Section III proposed a model-order reduction method base on the open-circuit suppression principle and the solution in the time domain is provided based on the vector fitting method combing with the backward difference method. In section IV, the proposed method is validated by comparing its simulation results with the ones calculated or measured in other papers. In section V, the integrated grounding system in the high-speed railway system is modeled and the direct lightning overvoltages of the catenary are simulated using the proposed method.

Modeling Method of the Thin-wire Structures

Modified Image Method

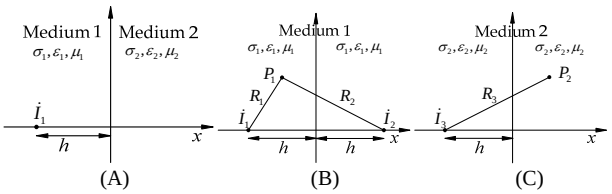

FIG. 1 PRINCIPLE DIAGRAM OF MODIFIED IMAGE METHOD.(A) CONFIGURATION OF THE MEDIUM AND THE SOURCE (B) THE SOURCE AND ITS IMAGE REPRESENTING THE FIELD IN MEDIUM 1 (C) AN IMAGE REPRESENTING THE FIELD IN MEDIUM 2

A current source $\dot{I}_1$ is located at a distance h from the interface of tow medium as shown in Fig. 1(A), in which the conductivity, permittivity and the permeability are σ_1 , ε_1 , μ_1 and σ_2 , ε_2 , μ_2,

respectively. A modified image current source $\dot{I}_2$ is introduced and the field in the medium 1 can be calculated using the superposition theorem, which is shown in Fig. 1(B). In order to calculate the field in the medium 2, another modified image $\dot{I}_3$ is introduced, as shown in Fig. 1(C). Both the value of the image current source can be evaluated according to the boundary condition.

Suppose ε_0 and ε as the permittivity of the air and the ground, σ as the conductivity of the ground, the value of the image current source $\dot{I}_2$ and $\dot{I}_3$ can be evaluated using the following equations.

Type I: Current source and the observation point both in the soil, the field can be evaluated as a sum of the field of the current source $\dot{I}_1$ and its image $\dot{I}_2$:

$$\dot{I}_2 = \frac{j\omega\varepsilon + \sigma - j\omega\varepsilon_0}{j\omega\varepsilon + \sigma + j\omega\varepsilon_0}\dot{I}_1 \tag{1}$$

Type II: Current source and the observation point both in the air, the field can be evaluated as a sum of the field of the current source $\dot{I}_1$ and its image $\dot{I}_2$:

$$\dot{I}_2 = \frac{j\omega\varepsilon_0 - j\omega\varepsilon - \sigma}{j\omega\varepsilon + \sigma + j\omega\varepsilon_0}\dot{I}_1 \tag{2}$$

Type III: Current source in the soil and the observation point in the air, the field can be evaluated as field due to the modified current source $\dot{I}_3$:

$$\dot{I}_3 = \frac{2\,j\omega\varepsilon_0}{j\omega\varepsilon + \sigma + j\omega\varepsilon_0}\dot{I}_1 \tag{3}$$

Type IV: Current source in the air and the observation point in the soil, the field can be evaluated as field due to the modified current source $\dot{I}_3$:

$$\dot{I}_3 = \frac{2(j\omega\varepsilon + \sigma)}{j\omega\varepsilon + \sigma + j\omega\varepsilon_0}\dot{I}_1 \tag{4}$$

PEEC Method

PEEC method is a full wave method for solving the conductor system based on electric-field integral equation, and a lumped circuit model can be obtained. Based on the principle of this method, the thin-wire structure can be viewed as a combination of short filament whose current density and charge density distribute along the conductor. The total tangential electric field shall be as (5).

$$\vec{s}\cdot\vec{E}^t(\vec{r}) = \vec{s}\cdot\left[\vec{E}^i(\vec{r}) + \vec{E}^s(\vec{r})\right] = \vec{s}\cdot\frac{\vec{J}(\vec{r})}{\sigma} \tag{5}$$

where, $\vec{s}$ is a unit tangential vector along the wire, $\vec{E}^i(\vec{r})$ is the incident electric field, $\vec{E}^s(\vec{r})$ is the scattered electric field which can be represented as (6).

$$\vec{E}^s(\vec{r}) = j\omega\vec{A}(\vec{r}) - \nabla\dot{\phi}(\vec{r}) \tag{6}$$

where, $\vec{A}(\vec{r})$ is the magnetic potential vector and $\dot{\phi}(\vec{r})$ is the electric scalar potential, whose expression equation is

$$\vec{A}(\vec{r}) = \frac{\mu}{4\pi}\int_c \vec{s}\cdot\dot{I}(\vec{r})\cdot\frac{e^{-\Gamma R}}{R}\cdot ds' \tag{7}$$

$$\dot{\phi}(\vec{r}) = \frac{1}{4\pi\varepsilon}\int_c \rho_l(\vec{r})\cdot\frac{e^{-\Gamma R}}{R}\cdot ds' \tag{8}$$

where, ds' is a element of the wire, $\Gamma = \sqrt{j\omega\mu(\sigma + j\omega\varepsilon)}$ is the propagation constant of the considered medium, the distance from the source and the observation point is $R = |\vec{r} - \vec{r}\,'|$.

Substituting (6), (7) and (8) into(5), (9) is obtained

$$\vec{s}\cdot\vec{E}^i(\vec{r}) - \vec{s}\cdot\frac{\dot{I}(\vec{r})}{\sigma_l} - j\omega\frac{\mu}{4\pi}\int_c \vec{s}\cdot\vec{s}'I(\vec{r}')\frac{e^{-\Gamma R}}{R}ds' - \frac{d\phi}{ds} = 0 \tag{9}$$

where σ_l is the conductivity of the conductor.

Considering a segment connecting with node *k* and *l*, and Integrating (9) along the segment from, (10) is obtained.

$$\begin{aligned}\dot{\phi}_{lk} = \dot{\phi}_l - \dot{\phi}_k = &-j\omega\frac{\mu}{4\pi}\int_{s'=k}^{s'=l}\int_c \vec{s}\cdot\vec{s}'I(\vec{r}')\frac{e^{-\Gamma R}}{R}ds'ds \\ &-\int_{s'=k}^{s'=l}\frac{\dot{I}(\vec{r}')}{\sigma_l}ds + \int_k^l \vec{s}\cdot\vec{E}^i(\vec{r})ds\end{aligned} \tag{10}$$

According to (10), the first term can be defined as the impedance of the along the conductor segment, which can be expressed as

$$Z_{Lmn} = -\frac{j\omega\mu}{4\pi}\int_{Lm}\int_{Ln}\frac{e^{-\Gamma R}\cos\varphi}{R}dl_n dl_m \tag{11}$$

Based on the conservation of charge, the charge density $\dot{\tau}_l$ can be expressed as

$$\dot{\tau}_l = \dot{I}_{Tk}/(j\omega L_k) \tag{12}$$

where, $\dot{I}_{Ti}$ is the leakage current and the L_k is the length of the *k*th segment. As a result, the average potential can be calculated using the following equations.

$$\dot{\phi}_k = \frac{1}{L_k}\int_{L_k}\dot{\phi}(\vec{r})dl_k = \frac{1}{4\pi(\sigma + j\omega\varepsilon)L_k}\int_{l_k}\int_c \frac{\dot{I}_{Ti}}{L_i}\times\frac{e^{-\Gamma R}}{R}dl_i dl_k \tag{13}$$

Let

$$\dot{\phi}_k = \sum_{i=1}^{M} Z_{Tki} \dot{I}_{Ti} \tag{14}$$

The horizontal impedance Z_{Tki} can be defined as

$$Z_{Tki} = \frac{1}{4\pi(\sigma + j\omega\varepsilon)L_k L_i} \int_{L_k}\int_{L_i} \frac{e^{-\Gamma R}}{R} dl_i dl_k \tag{15}$$

As we can see, the form of Z_{Tki} is the same with Z_{Lmn}, which can be calculated using Neman integration or numerical method.

Multi-port Macromodel of the Complex Thin-wire Structures

Model-order Reduction Method based on the Open-circuit Suppression Method

A thin-wire conductor system can be viewed as a number of cells composed of straight filaments, whose PEEC circuit is shown as Fig. 2.

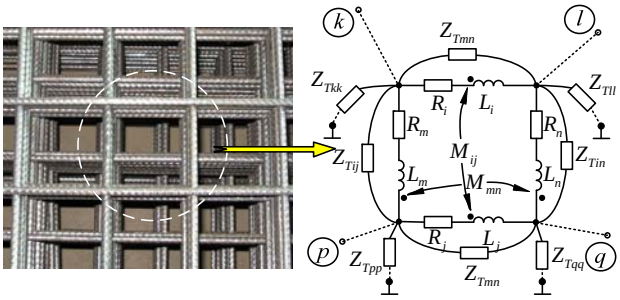

FIG. 2 THIN-WIRE STRUCTURE AND ITS EQUIVALENT CIRCUIT

According to a certain filament *k* connecting between the node *i* and *j*, whose electric potentials $\dot{\phi}_k$ can be expressed by (16) because the length of the filament is short enough.

$$\dot{\phi}_k = \frac{\dot{U}_{ni} + \dot{U}_{nj}}{2} \tag{16}$$

where, $\dot{U}_{ni}$ and $\dot{U}_{nj}$ is the node voltage of node i and j, respectively. Considering all of the filaments in the conductor system, the relation between the filament electric potential and the node voltage can be written as

$$\dot{\boldsymbol{\phi}} = 0.5 \times abs(\mathbf{A}^T) \cdot \dot{\mathbf{U}}_n = \mathbf{P} \cdot \dot{\mathbf{U}}_n \tag{17}$$

where, $\mathbf{A}$ is the incidence matrix in the node voltage method, the function $abs(\cdot)$ denotes to a calculation of the element's absolute value in the corrsponding matrix.

Based on the node voltage method, the node admittance matrix considering only the axial direction impedance can be expressed as (18).

$$\mathbf{Y}_{nRL} = \mathbf{A} \cdot \mathbf{Z}_b^{-1} \cdot \mathbf{A}^T \tag{18}$$

where $\mathbf{Z}_b$ axial direction impedance.

Meanwhile，the leakage current can be described by the leakage admittance matrix and the relation equation between the filament electric potential and the leakage current is

$$\dot{\mathbf{I}}_b = \mathbf{Y}_b \cdot \dot{\boldsymbol{\phi}} \tag{19}$$

where, $\mathbf{Y}_b$ is the leakage admittance matrix, which can be obtained by $\mathbf{Y}_b = \mathbf{Z}_{T_{ki}}^{-1}$.

Assuming the leakage current flowing from the two nodes of each filament which is equal to each other, the relation equation of the leakage current and the node current can be written as (20)

$$\dot{\mathbf{I}}_n = 0.5 \times abs(\mathbf{A}) \cdot \dot{\mathbf{I}}_b = \mathbf{Q} \cdot \dot{\mathbf{I}}_b \tag{20}$$

Based on the Kirchhoff's circuit laws, the equations of the circuit can be obtained, as shown in (21).

$$\mathbf{Y}_{nRL} \cdot \dot{\mathbf{U}}_n = \dot{\mathbf{I}}_s - \dot{\mathbf{I}}_n \tag{21}$$

where, $\dot{\mathbf{I}}_s$ denotes to the incident current vector of the current source. Substituting (18), (19) and (20) into (21), the equations corresponding to the node voltage method is

$$\left(\mathbf{A} \cdot \mathbf{Z}_b^{-1} \cdot \mathbf{A}^T + \mathbf{Q} \cdot \mathbf{Y}_b \mathbf{Q}^T\right) \cdot \dot{\mathbf{U}}_n = \dot{\mathbf{I}}_s \tag{22}$$

Let $\mathbf{Y}_n = \mathbf{A} \cdot \mathbf{Z}_b^{-1} \cdot \mathbf{A}^T + \mathbf{Q} \cdot \mathbf{Y}_b \mathbf{Q}^T$, and $\mathbf{Y}_n$ is the node admittance matrix of the whole network.

For a thin-wire system with a large number of conductors, the order of the node admittance matrix would be very large which would result in an inefficient computation. In this section, the open-circuit suppression principle is used to reduce the order of the model.

The nodes in the conductor system can be divided into two types according to the different location of the nodes, one kind is the node connecting to the external circuit and another is internal nodes. Because the internal nodes would not connect to the external circuit, they can be eliminated to reduce the order of the model.

Let the voltage and current vector of the internal nodes are $\dot{\mathbf{U}}_2$ and $\dot{\mathbf{I}}_2$, the voltage and current vector of the internal nodes are $\dot{\mathbf{U}}_1$ and $\dot{\mathbf{I}}_1$. Rearrange (22) as

$$\begin{bmatrix}\dot{\mathbf{I}}_{s1}\\ \dot{\mathbf{I}}_{s2}\end{bmatrix}=\begin{bmatrix}\mathbf{Y}_{11} & \mathbf{Y}_{12}\\ \mathbf{Y}_{21} & \mathbf{Y}_{22}\end{bmatrix}\begin{bmatrix}\dot{\mathbf{U}}_{n1}\\ \dot{\mathbf{U}}_{n2}\end{bmatrix} \tag{23}$$

Considering the incident current of the internal nodes $\dot{\mathbf{I}}_{s2}=\mathbf{0}$, so the second equation of (23) can be written as

$$\mathbf{Y}_{21}\dot{\mathbf{U}}_{n1}+\mathbf{Y}_{22}\dot{\mathbf{U}}_{n2}=\mathbf{0} \tag{24}$$

and the node voltage of the internal nodes can be expressed by the node voltage of the external nodes, as shown in (25).

$$\dot{\mathbf{U}}_{n2}=-\mathbf{Y}_{22}^{-1}\mathbf{Y}_{21}\dot{\mathbf{U}}_{n1} \tag{25}$$

Substituting (25) into the first equation of (23), the equations of the external nodes can be obtained.

$$\dot{\mathbf{I}}_{1}=\left(\mathbf{Y}_{11}-\mathbf{Y}_{12}\mathbf{Y}_{22}^{-1}\mathbf{Y}_{21}\right)\dot{\mathbf{U}}_{n1} \tag{26}$$

From equation (26), a new node admittance matrix is obtained, as shown in (27). Because the number of the external nodes is much less comparing with the number of the total nodes, the order can be reduced effectively.

$$\mathbf{Y}'=\mathbf{Y}_{11}-\mathbf{Y}_{12}\mathbf{Y}_{22}^{-1}\mathbf{Y}_{21} \tag{27}$$

Time Domain Solution of the Macromodel

For the purpose of simplicity, a simple grounding system is used to represent the mathematical derivation of the solution of the macromodel, as Fig. 3.

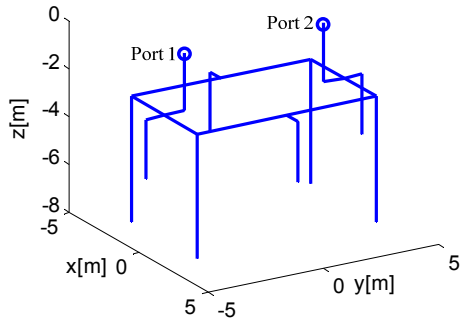

FIG. 3 SIMPLIFIED GROUNDING SYSTEM

Step 1: Based on the method of previous section, the node admittance matrix can be obtained and it can be fitted using the vector fitting method, as shown in (28).

$$\mathbf{Y}=\begin{bmatrix}Y_{11}(s) & Y_{12}(s)\\ Y_{21}(s) & Y_{22}(s)\end{bmatrix}=\begin{bmatrix}\sum_{i=1}^{NF}\frac{c_{11,i}}{s-p_i}+d_{11} & \sum_{i=1}^{NF}\frac{c_{12,i}}{s-p_i}+d_{12}\\ \sum_{i=1}^{NF}\frac{c_{21,i}}{s-p_i}+d_{21} & \sum_{i=1}^{NF}\frac{c_{22,i}}{s-p_i}+d_{22}\end{bmatrix} \tag{28}$$

Step 2: Using the Laplace inverse transformation, the time domain equation can be obtained, shown in (29)

$$\sum_{i=0}^{NF}\begin{bmatrix}a_i & 0\\ 0 & a_i\end{bmatrix}\begin{bmatrix}\frac{d^i u_1}{dt^i}\\ \frac{d^i u_2}{dt^i}\end{bmatrix}=\sum_{i=0}^{NF}\begin{bmatrix}b_{11,i}+d_{11}\cdot a_i & b_{12,i}+d_{12}\cdot a_i\\ b_{21,i}+d_{11}\cdot a_i & b_{22,i}+d_{11}\cdot a_i\end{bmatrix}\begin{bmatrix}\frac{d^i i_1}{dt^i}\\ \frac{d^i i_2}{dt^i}\end{bmatrix} \tag{29}$$

Step 3: Making use of the backward differentiation formula to approximates the time derivatives, the

$$\begin{aligned}&\sum_{i=0}^{NF}\begin{bmatrix}a_i & 0 & -c_{11,i} & -c_{12,i}\\ 0 & a_i & -c_{21,i} & -c_{22,i}\end{bmatrix}\cdot\Delta t^{NF-i}\cdot\mathbf{x}^{n+1}\\ &=-\sum_{i=1}^{NF}\begin{bmatrix}a_i\cdot B_\omega(i,:) & 0 & -c_{11,i} & -c_{12,i}\\ 0 & a_i\cdot B_\omega(i,:) & -c_{21,i} & -c_{22,i}\end{bmatrix}\cdot\Delta t^{NF-i}\cdot\mathbf{x}^{his}\end{aligned} \tag{30}$$

where,

$$B_\omega=\begin{bmatrix}\omega_{NF}(NF) & \omega_{NF-1}(NF) & \omega_{NF-2}(NF) & \cdots & \omega_1(NF)\\ 0 & \omega_{NF-1}(NF-1) & \omega_{NF-2}(NF-1) & \cdots & \omega_1(NF-1)\\ \vdots & \vdots & \vdots & \vdots & \vdots\\ 0 & 0 & 0 & \cdots & \omega_1(1)\end{bmatrix}$$

, $\omega_j(p)=(-1)^j\cdot\binom{p}{j}$, which is a cumulative sum function, $\mathbf{x}^{his}=\left[\mathbf{u}_1^{his}\ \ \mathbf{u}_2^{his}\ \ \mathbf{i}_1^{his}\ \ \mathbf{i}_2^{his}\right]^T$, in which $\mathbf{u}_1^{his}=\left[u_1^{n-NF+1}\ \cdots\ u_1^{n}\right]$, $\mathbf{u}_2^{his}=\left[u_2^{n-NF+1}\ \cdots\ u_2^{n}\right]$, $\mathbf{i}_1^{his}=\left[i_1^{n-NF+1}\ \cdots\ i_1^{n}\right]$, $\mathbf{i}_2^{his}=\left[i_2^{n-NF+1}\ \cdots\ i_2^{n}\right]$, and $\mathbf{x}^{n+1}=\left[u_1^{n+1}\ \ u_2^{n+1}\ \ i_1^{n+1}\ \ i_2^{n+1}\right]^T$. Combined with the boundary conditions of the model, a transient analysis can be accomplished.

Validation of the Method in Thin-wire Structure System Transient Analysis

Transient Analysis of a Vertical Conductor above the Ground

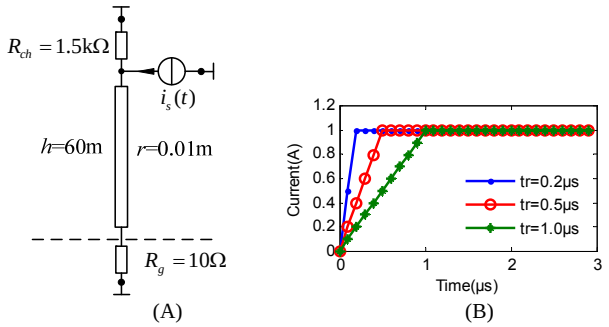

FIG. 4 CALCULATIONAL MODEL OF A VERTICAL CONDUCTOR INJECTED AT THE TOP BY A STEP CURRENT SOURCE. (A) CALCULATION MODEL (B) INJECTED CURRENT SOURCE

The calculation model consists of a 60m high vertical conductor connected to a grounding resistance of 10Ω

at its bottom and to a surge impedance of 1500Ω at its top, which is shown in Fig. 4(A). A step current was assumed to be injected at the top of the conductor. Three different front times were considered, namely t_f =0.2μs, t_f=0.5μs and t_f=1μs, as shown in Fig. 4(B).

Transient voltages at the top of the vertical conductor according to different front times are calculated using the macromodel proposed in this paper, as shown in the left side of Fig. 5, and the corresponding results published in Alberto D. Conti's paper are shown in the right side. It is shown that the all of the results match well with each other, which demonstrates the accuracy of this method for dealing with the transient analysis of the vertical conductor.

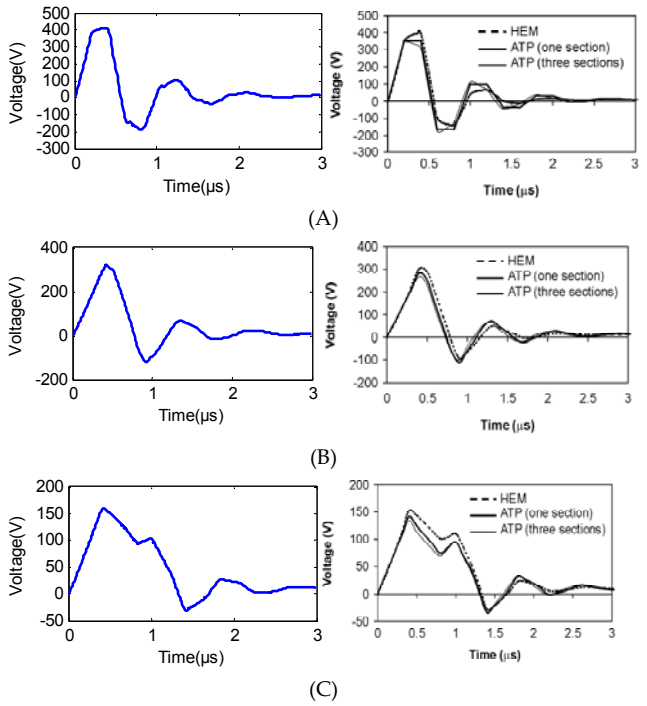

FIG. 5 VOLTAGES AT THE TOP OF THE VERTICAL CONDUCTOR. (A) RESULTS ACCORDING TO t_f=0.2μs (B) RESULTS ACCORDING TO t_f=0.5μs (C) RESULTS ACCORDING TO t_f=1μs.

Transient Analysis of a Vertical Conductor System above the Ground

A vertical conductor system of four parallel vertical conductors with 16.5 mm radium is shown in Fig. 6. This is the same configuration carried out by Hara. The vertical conductors are excited by a pulse generator (PG) through a current lead wire, and the top voltage is defined as the voltage between the conductor top and a measuring wire. In the simulation, the resistivity of the earth was set to 1.69×10^{-8} Ω·m, PG was modeled by a current source with 5kΩ internal resistance, whose waveform is shown in Fig. 7.

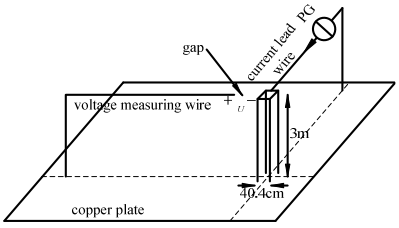

FIG. 6 CONFIGURATION OF A VERTICAL CONDUCTOR SYSTEM EVALUATED BY HARA

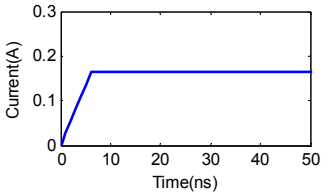

FIG. 7 WAVEFORM OF THE CURRENT SOURCE

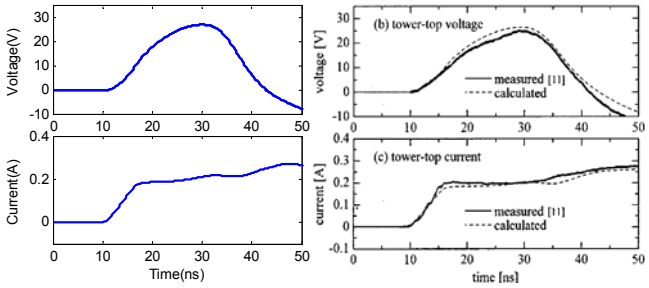

FIG. 8 VOLTAGE AND CURRENT CALCULATED AND MEASURED AT THE TOP OF THE VERTICAL CONDUCTOR SYSTEM. (A) CALCULATED RESULTS (B) MEASURED BY HARA

The waveforms of the tower-top voltage and current are shown in FIG. 8 (A). The results measured by Hara are given in Fig. (B). Both the results agree well with measured ones which demonstrate the validity of the macromodel proposed in this paper.

Transient Analysis of a Grounding Grid

A 60×60m² grounding grid with 6 by 6 10 meter square meshes, 10m ground rods in the corners constructed of copper conductors with diameter 1.4cm, is buried at 0.6m depth, as shown in FIG. 9. The soil's resistivity and relative permittivity is 100 Ω·m and 36, respectively. A 1/20μs 1kA crest current surge is injected at the middle point of the grid.

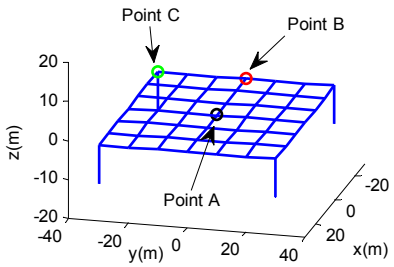

FIG. 9 GROUNDING GRIDS IN THE SIMULATION

Transient voltages at the feeding point A, middle point B and corner point C are presented in Fig. 10(A). Results calculated by Grcev Leonid D. are illustrated in Fig. 10(B). The good agreement between the compared results has been achieved.

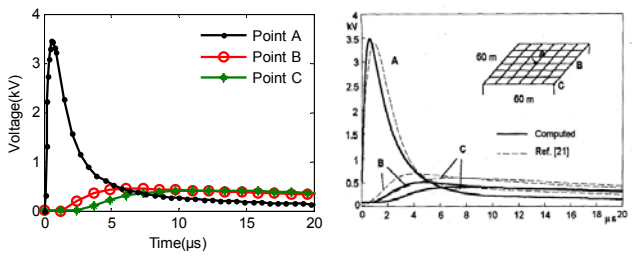

FIG. 10 COMPUTED TRANSIENT POTENTIAL AT THREE POINTS ON THE GROUNDING GRID (A) POTENTIAL OF A, B AND C CALCULATED BY PEEC (B) RESULTS CALCULATED GRCEV LEONID D.

Applications

Because the viaduct structure are widely adopted in the China's high-speed railway system, the increase of the height of the catenary's overhead lines will lead to a frequent lightning striking. Nowadays, there is no ground wire equipped above the power supply lines whose geometry is shown in Fig. 11, which may result in a serious lightning accident. In order to represent the effect of the ground wire and evaluate of the withstand level of the catenary, the integrated grounding system is modeled and the lightning overvoltage of the catenary is calculated.

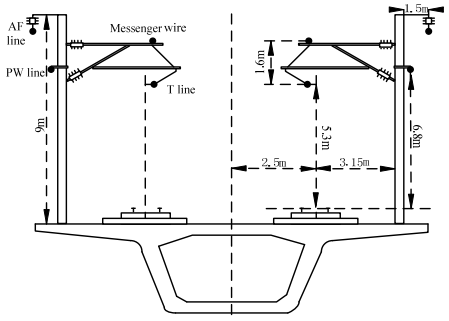

FIG. 11 GEOMETRY OF CATENARY IN THE HIGH-SPEED RAILWAY SYSTEM

Structure of the Integrated Grounding System of the Viaduct in High-speed Railway

The structure of the integrated grounding system of the viaduct is shown in Fig. 12, in which there are 6 grounding reinforcing bars are located on the surface of the box girder and 2 vertical grounding reinforcing bars are use to connect the box girder and the pier, meanwhile, the structural reinforcing bars can also be used as the grounding conductors in principle. The grounding sticks at the corner the pile cap are adopted as the grounding rod and their length are 5~30m in general. The cross section area of the reinforcing bars should not less than 200mm^2.

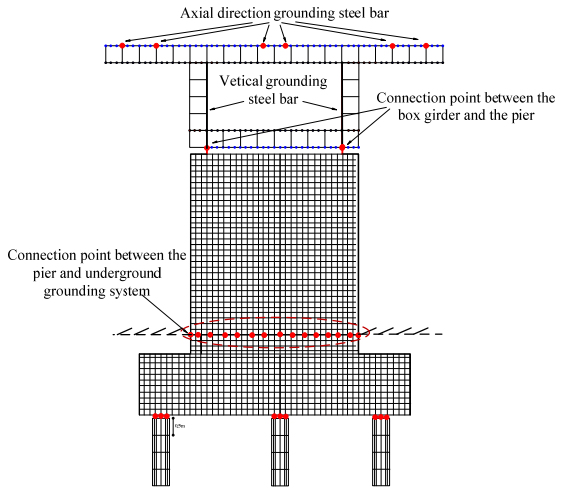

FIG. 12 STRUCTURE OF THE INTEGRATED GROUNDING SYSTEM OF THE VIADUCT

Macromodel of the Integrated Grounding System of the Viaduct in High-speed Railway

Because of the complex structure of the integrated grounding system, it is divided into three sections in this paper, they are the grounding system of the box girder, the grounding system of the pier above the ground and the grounding system underground, as shown in Fig. 13.

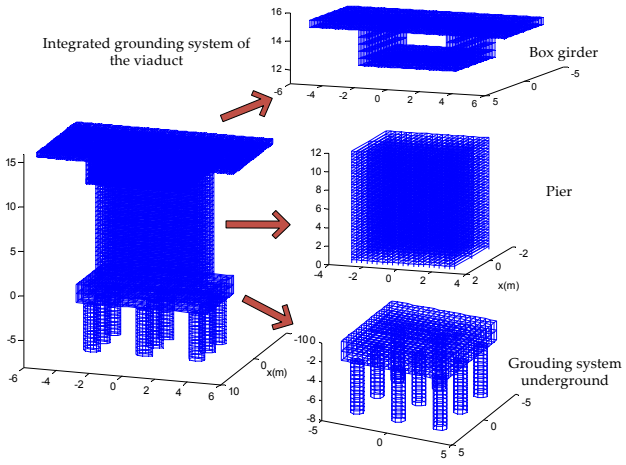

FIG. 13 MODELING OF THE INTEGRATED GROUNDING SYSTEM OF VIADUCT

Using the macromodeling method proposed in this paper, the multi-port macromodel of each section can be obtained and the whole model can be built according to the connection point of the integrated grounding system, which is shown in Fig.14.

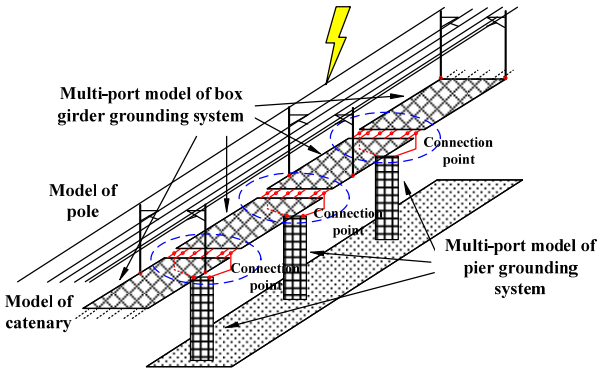

FIG. 14 EQUIVALENT NETWORK OF THE INTEGRATED GROUNDING SYSTEM OF VIADUCT

The overhead lines of the catenary can be modeled as a multi-conductor transmission line system, combined with the multi-port macromodel of the integrated grounding system, the lightning overvoltage is calculated due to a 1kA 2.6/50 μs lightning current directly striking at the ground wire. The voltages of the power supply line's insulator are shown in Fig. 15, in which the resistivity of the ground is 100 Ω·m, and the withstand level of the catenary are listed in Table 1 with different ground resistivity.

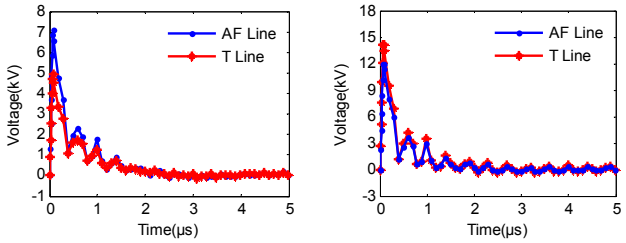

FIG. 15 POTENTIALS OF THE AF LINE AND T LINE AND VOLTAGES OF THE INSULATOR OF AF LINE AND T LINE (HEIGHT OF THE VIADUT IS 8M, DEPTH OF THE GROUNDING STICK IS 8M AND EARTH RESISTIVITY ($\rho = 100\Omega \cdot m$). (A) POTENTIALS OF THE AF LINE AND T LINE (B) VOLTAGES OF THE INSULATOR OF AF LINE AND T LINE

TABLE 1 LIGHTNING WITHSTAND LEVEL OF AF LINE AND T LINE DUE TO LIGHTNING STRIKING ON GROUND WIRE

Resistivity of the ground (Ω·m)	100		500		1000	
Catenary's line	AF	T	AF	T	AF	T
Withstand level (kA)	58.79	58.13	58.50	57.83	58.49	57.81

The lightning withstand levels of AF line and T line show little difference with different ground resistivity, that is because the large number of the grounding conductors resulting in a good grounding effect.

In order to represent the effect of the ground wire, the overvoltage due to a direct lightning striking to AF line and T line are also calculated and the withstand levels are shown in Table 2. It can be concluded that the equipment of the ground wire can reduce the overvoltage effectively, which will improve the reliability of the power supply in the high-speed railway system.

TABLE 2 LIGHTNING WITHSTAND LEVEL OF AF LINE AND T LINE DUE TO LIGHTNING STRIKING ON AF LINE AND T LINE

Catenary's line	AF	T
Withstand level (kA)	1.79	3.49

Conclusions

A time domain multi-port macromodeling method of the complex thin-wire system is proposed in this paper. Based on the method, a circuit with low order can be achieved and a time domain numerical solution method is provided which can ensure the convergence of the model. The accuracy of the proposed method has been validated by comparing the results with the simulation or measurement results published in other papers.

ACKNOWLEDGMENT

This research was supported in part by National Natural Science Foundation of China under Grant No. 51177048, Natural Science Foundation of Hebei Province under Grant No. E2012502009, the Fundamental Research Funds for the Central Universities under Grant No. 11MG36, and the Fundamental Research Funds for the Hebei Province Universities under Grant No. Z2011220, respectively.

REFERENCES

Alberto De Conti, Silverio Visacro, Amilton Soares, Macro Aurelio O. Schroeder. "Revision, extension, and validation of Jordan's formula to calculate the surge impedance of vertical conductors." IEEE Transactions on Electromagnetic Compatibility, 48.3 (2006): 530-536.

Baba Yoshihiro, Naoto Nagaoka, and Akihiro Ametani. "Modeling of thin wires in a lossy medium for FDTD simulations." IEEE Transactions on Electromagnetic Compatibility, 47.1 (2005): 54-60.

Baba Yoshihiro, Naoto Nagaoka, Akihiro Ametani. "FDTD simulation of a horizontal grounding electrode and modeling of its equivalent circuit." IEEE Transactions on Electromagnetic Compatibility, 48.4 (2006): 817-825.

Leonid D. Grcev, and Dawalibi Farid. "An electromagnetic model for transients in grounding systems." Power

Delivery, IEEE Transactions on 5.4 (1990): 1773-1781.

Leonid D. Grcev. "Computer analysis of transient voltages in large grounding systems." IEEE Transactions on Power Delivery, 11.2 (1996): 815-823.

Leonid D. Grcev, and Heimbach Markus. "Frequency dependent and transient characteristics of substation grounding systems." IEEE Transactions on Power Delivery, 12.1 (1997): 172-178.

Noda Taku, and Shigeru Yokoyama. "Thin wire representation in finite difference time domain surge simulation." IEEE Transactions on Power Delivery, 17.3 (2002): 840-847

P. Yutthagowith, Akihiro Ametani, Naoto Nagaoka, Baba Yoshihiro. "Application of the partial element equivalent circuit method to analysis of transient potential rises in grounding systems." IEEE Transactions on Electromagnetic Compatibility, 53.3 (2011): 726-736

Shunchao Wang, Jinliang He, Bo Zhang, Rong Zeng, Zhanqing Yu. "A time-domain multiport model of thin-wire system for lightning transient simulation." IEEE Transactions on Electromagnetic Compatibility, 52.1 (2010): 128-135.

Shunchao Wang, Jinliang He, Bo Zhang, Rong Zeng. "Time-Domain Simulation of Small Thin-Wire Structures Above and Buried in Lossy Ground Using Generalized Modified Mesh Current Method." IEEE Transactions on Power Delivery, 26.1 (2011): 369-377

S. Visacro, A. Soares. "HEM: A model for simulation of lightning-related engineering problems." IEEE Transactions on Power Delivery, 20.2 (2005): 1206-1208.

T. Hara, O. Yamamoto, M. Hayashi, C. Uenoson,. "Empirical formulas of surge impedance for single and multiple vertical cylinder." IEE Japan Transactions 110 (1990): 129-137.

Yohei Taniguchi, Baba Yoshihiro, Naoto Nagaoka, Akihiro Ametani. "An Improvement of a Thin Wire Representation for FDTD Electromagnetic and Surge Calculations." IEEJ Transactions on Power and Energy 129 (2009): 198-204.

Xin Liu was born in Tianjin, China, in 1980. He received the B.S. degree from North China Electric Power University (NCEPU), Baoding, Hebei, China, in 2003, and M.S degree from Huazhong University of Science and Technology (HUST), Wuhan, Hubei, China, in 2006.

He is currently a Lecturer of electrical and electronic engineering at NCEPU, Baoding, Heibei, China and working toward the Ph.D. degree at NCEPU, Beijing, China. His research interests include electromagnetic compatibility (EMC) on power systems, electromagnetic pulse (EMP) interaction with transmission lines, and high-voltage equipment modeling.

Xiang Cui was born in Baoding, China, in 1960. He received the B.Sc. and M.Sc. degrees in electrical engineering from North China Electric Power University (NCEPU), China, in 1982 and 1984, respectively, and the Ph.D. degree in accelerator physics from China Institute of Atomic Energy, China, in 1988.

He is currently a Professor and the Head of the Electromagnetic Fields and Electromagnetic Compatibility Laboratory at NCEPU. He is the author or co-author of more than 200 journal articles. His current research interests include computational electromagnetics, electromagnetic environment and electromagnetic compatibility in power systems, insulation and magnetic problems in high voltage apparatus.